Solid state generators and energy harvesters for waste heat recovery and thermal energy harvesting

D. Zabek[a,*], F. Morini[b]

[a] *Institute of Heat Engineering, Warsaw University of Technology, ul Nowowiejska 21/25, 00-665 Warsaw, Poland*
[b] *GREMAN UMR 7347, Université de Tours, CNRS, 16 rue Pierre et Marie Curie, 37071 Tours, Cedex 2, France*

A B S T R A C T

This review covers solid state thermal to electrical energy converters capable of transforming low grade heat directly into electricity for waste heat recovery and thermal energy harvesting. Direct solid state heat engines, such as thermoelectric modules and thermionic converters for spatial temperature gradients, are compared with pyroelectric energy harvesters and thermomagnetic generators for transient changes in temperature. Temperature and size limitations along with the maturity of the technologies are discussed based on energy density and temperature range for the different generator technologies. Despite the low energy conversion efficiency with solid state generators, electric power density ranges from $4\,nW/mm^2$ to $324\,mW/mm^2$. The most promising sector to implement changes while reducing the primary energy consumption and saving resources, is the processing industry along with stationary and mobile electronics.

1. Introduction

The constant growth in population is followed by an increasing demand in electrical energy, since our health, safety, and comfort relies on a continuous generation and distribution of electric power. Due to the volatile nature of electricity and the limited ability of storing electrical energy, a continuous energy generation is needed. Currently over 76% of all electrical energy is generated from non-renewable energy sources with heat remaining the primary driver [1]. Heat is utilized in conventional internal and external combustion cycles which are widely optimized in terms of non-renewable energy sources and limited by environmental regulations. At the same time, conventional combustion cycles expel large amounts of low grade thermal energy and waste heat. Waste energy, if it can be captured or harvested, is a renewable or sustainable energy source which can be used for co-generation and energy harvesting. In addition, large quantities of currently unexplored heat sources are readily available for waste heat recovery and thermal energy harvesting; including e.g. solar radiation energy, geothermal energy, and thermal energy expelled by the processing industry (aluminium melting, glass manufacture, oil and gas, as well as paper and cement production) or the building environment (air conditioning and refrigeration) [2–4]. Solar radiation energy is a particularly important and an infinite source of renewable energy with an exceptionally high power density.

Fig. 1 compares the source power densities for various ambient thermal and radiation energy sources before conversion [5]. Thermal energy sources in solid (e.g. ground heat), liquid (e.g. hot springs) and gaseous (e.g. airflow) phases have a low power density of around $10\,\mu W/cm^3$ in contrast to direct and indirect radiation energy sources with a high power density of up to $10\,000\,\mu W/cm^2$, which can be directly utilized for thermal to electrical energy conversion. However, despite the high power density of direct and indirect radiation sources the temperatures are below 230 °C and therefore are considered too low for conventional thermal to electric energy conversion systems [6]. In addition, conventional energy conversion systems, such as Bryton or Rankine cycles, have scaling issues at low temperatures and small heat loads, for which reason practical applications need a minimum generator size of 1 kW [7]. In an effort to utilize small heat sources below 1 kW a number of small-scale solid state thermal to electrical energy converters have been developed, capable of converting low temperature heat directly into electrical energy. Solid state thermal to electrical energy converters are heat engines, or small generators, and energy harvesters capable of transforming heat directly into electricity. The governing physical principles with solid state thermal to electrical energy converters work over several orders of magnitude and enable the utilization of previously unexplored low grade thermal energy and waste heat. With solid state heat engines, small quantities of low grade thermal energy and waste heat, at temperatures just above ambient, can

---

Nomenclature

A	surface area, m^2
A*	Richardson constant for semiconductors, 1
A_C	empirical constant for thermomagnetic generators, 1
A_R	Richardson constant for metals, $A.m^{-2}.K^{-2}$
B	magnetic flux density, T
d	distance, m
E	energy, J
F_E	pyroelectric figure of merit, 1
H	total magnetic field, $A.m^{-1}$
I	electrical current, A
J	total current density, $A.m^{-2}$
J_C	current density from the cold electrode to the hot electrode, $A.m^{-2}$
J_H	current density from the hot electrode to the cold electrode, $A.m^{-2}$
k_B	Boltzmann constant, $8.61733\ eV.K^{-1}$
L	shunt length, m
N	number of turns, 1
n_o	turns per unit length of the inductor coil, m^{-1}
P	electrical power generated, W
$P_{Polarization}$	polarization, $C.m^{-2}$
p*	pyroelectric coefficient, $C.m^{-2}.K^{-1}$
Q	heat load, J
Q'	dissipated thermal power by the electron flow, $W.m^{-2}$
Q'_R	dissipated thermal power by radiation, $W.m^{-2}$
q	elementary charge, $1.60218 \times 10^{-19}\ C$
S	average area enclosed by the inductor coil, m^2
$S_{Seebeck}$	seebeck coefficient, $V.K^{-1}$
T	temperature or average temperature, K
T_c	Curie temperature, K
T_{Cold}	temperature of the cold electrode, K
T_{Hot}	temperature of the hot electrode, K
V	electrical potential, V
zT	thermoelectric figure of merit, 1
$\Delta P_{Polarization}$	change in polarization, $C.m^{-2}$
ΔT	temperature difference, K or °C
Δt	time difference, s
dB	change on the magnetic field flux, Tesla or Gauss
εC	emissivity of the cold electrode material, 1
εH	emissivity of the hot electrode material, 1
Φ	work function, eV
κ	thermal conductivity, $W.m^{-1}.K^{-1}$
H	total magnetic field [A/m]
η_{Carnot}	Carnot efficiency, 1
η_{TE}	thermoelectric efficiency, 1
$\eta_{Thermionic}$	thermionic efficiency, 1
$\eta_{Pyroelectric}$	pyroelectric efficiency, 1
$\eta_{Thermomagnetic}$	thermomagnetic efficiency, 1
ρ	electrical resistivity, $\Omega.m$
ε	relative dielectric permittivity, 1
μ_r	relative magnetic permeability, 1
μ_r	permeability of free space, $4\pi.10^{-7}\ H.M$
σ_{SB}	$5.67036 \times 10^{-8}\ W \cdot m^{-2} \cdot K^{-4}$
η	experimental efficiency, 1

be directly converted into electrical power in the *microwatt* to *milliwatt* range. The generated electrical power allows to locally power a large number of small scale electronic devices as well as autonomous and self-sustaining applications, without the need for maintenance and additional costs. Most autonomous and self-sustaining applications such as low power electronics, internet of the things (IoT) devices and wireless sensor networks [8] or mechanical actuators and pump applications[9], can be powered using solid state energy converters. The power level with low power electronics is usually in the range between 10 nW and 1 mW when operating continuously or intermittently, and can be used without the need for external batteries or hard wiring [10,11]. In addition, solid state energy converters do not have any mechanical motion when converting heat directly into electrical energy, for which reason no mechanical wear and fewer transformation losses are expected. A recent review provides more general information on materials, methods and devices for thermal energy harvesting [12]. However, this review compares currently available industrial applications as well as experimental and practical small-scale solid state

thermal to electrical energy conversion technologies capable of recovering low grade waste heat. Amongst the most popular solid state heat engines are commercially available thermoelectric modules utilizing a spatial temperature differences between a static heat source and heat sink. A spatial temperature difference can be also utilized using experimental thermionic devices transforming a constant heat flow directly into electricity. In contrast to spatial temperature difference, transient or oscillating changes in temperature, such as day and night time temperature changes, introduce fluctuating heat flows. A fluctuating heat flow can be converted into electrical energy using solid state pyroelectric energy harvesters or thermomagnetic devices, which show interesting developments in recent years. The development of heat engines over time has also revealed some highly innovative concepts for solid state generators such as the single atom engine [13], thermal resonators using thermal effusivity materials [14] or more abstract approaches such as a magnon-driven quantum-dot heat engine [15]. Further, chemical principles such as thermogalvanic converters [16] using alkali metals [17], are currently of more interest from a theoretical point of view when used for waste heat recovery and thermal energy harvesting applications. However, this review predominantly focuses on experimental and practical applications of solid state heat engines for waste heat recovery and thermal energy harvesting. When recovering heat and harvesting thermal energy, every thermal energy conversion process is limited by the Carnot energy conversion efficiency η_{Carnot} which is defined by the available heat source temperature T_{Hot} and heat sink temperature T_{Cold} as follows [18]:

$$\eta_{Carnot} = 1 - \frac{T_{Cold}}{T_{Hot}} \tag{1}$$

With a waste heat source temperature of 230 °C (503 K) and an ambient heat sink temperature of 22 °C (295 K), the maximum energy conversion efficiency of a generator or harvester is then limited to the Carnot efficiency of 41% (Eq. (1)). However, with decreasing heat source temperatures the Carnot efficiency also rapidly decreases due to a slower heat flow; this necessitates larger heat transfer equipment
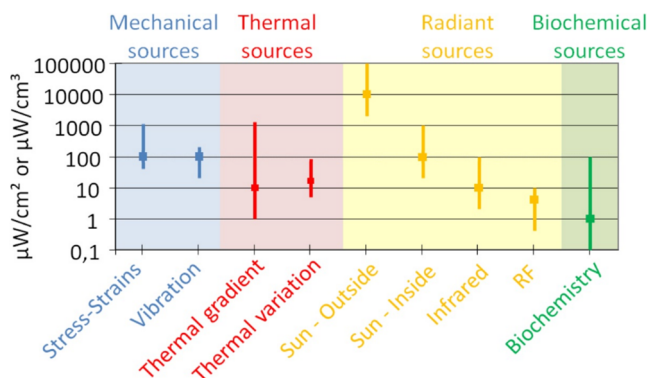

Fig. 1. Ambient source power densities before conversion (modified from [5]).

leading to more temperature sensitive generators. Hence, most practical waste heat recovery and thermal energy harvesting applications have a significantly smaller conversion efficiency, when compared to the theoretical Carnot efficiency, ranging from < 1% to 16% [19]. Regardless of the low efficiency, most ambient and small scale heat sources are readily available, for which reason the recovery of waste heat is considered free because operation costs are nearly zero. Therefore, only the electric output of the generator or energy harvester is of interest in practical applications. For this reason, this review compares current experimental and industrial advances in waste heat recovery and thermal energy harvesting technologies, along with the material engineering research efforts and recent generator designs. In detail, experimental and commercially available thermoelectric generators, thermionic converters, pyroelectric harvesters, thermomagnetic generators and the materials employed are discussed. The theoretical and the experimental efficiency η along with the available electrical energy are compared based on the effective electric output, power density, and output voltage/current. In this analysis the experimental efficiency η is defined by the electric output and the heat input as follows:

$$\eta = \frac{Electric\ output}{Heat\ input} \tag{2}$$

With a clear focus on the available heat source temperature, this review maps the available solid-state generator technologies and discusses industrial and experimental applications for waste heat recovery and thermal energy harvesting. When implementing waste heat recovery and thermal energy harvesting applications, generators size limitation and scaling issues are also discussed. In addition, the maturity and the costs of the waste heat recovery technologies and their applications are compared, followed by an outlook for prospective opportunities in these fields. Considering that the electric output power of the generator or harvester is free, this research can be paralleled with the effort to reduce the demand for primary energy sources and enable an autonomous powering of practical low power applications, without the need for external batteries, hard wiring and maintenance. The sectors benefitting most from waste heat recovery and energy harvesting applications and the reduction of primary energy consumption and conservation of resources, is the processing industry followed by stationary and mobile electronics.

2. Thermoelectric generators

Thermoelectric devices, or thermoelectric generators (TEG), are solid state heat engines and convert thermal energy directly into electrical energy. Thermal energy from a hot heat source and a cold heat sink creates a spatial temperature difference which can be utilized in a TEG. When the TEG is place between the hot heat source and a cold heat sink, the temperature difference is converted into an electric current across the generator terminals. This effect is based on the thermoelectric, or Seebeck, effect. The Seebeck effect describes the voltage developed across two dissimilar electrical conductor materials creating a hot thermoelectric junction. The assembly of thermoelectric junctions is known as a TEG module and acts as an electric power generator continuously driving a direct electric current (DC) through an external electrical load.

Fig. 2 shows a cross section schematic of a TEG module with a hot side (T_{Hot}) heated by the heat source (Q_{in}) and a cold side (T_{Cold}) cooled by the heat sink (Q_{out}). At the hot side, the TEG architecture has a connection, or junction, which electrically joins two dissimilar semiconductor compounds [20]. One compound contains positive (p-) type charge carriers (holes) and the other compound contains negative (n-) type charge carriers (electrons). The two semiconductor compounds are electrically connected in series forming two electric TEG terminals. When the thermoelectric p-n junction is heated, an electrical potential difference (V) develops across the two TEG terminals in response to the applied temperature difference ($T_{Hot} - T_{Cold}$). The potential difference

is proportional to the applied temperature difference ΔT with most thermoelectric materials ranking around $\pm$ 200 µV/K [21]. When the two TEG terminals are connected to an external load, the terminal voltage discharges from the n-type terminal to the p-type terminal driving an electric current, based on the principle of drift diffusion, and therefore the TEG continuously converts thermal energy directly into electric power. If an external electric power is supplied to the thermoelectric module, the converse refrigeration effect, known as the Peltier effect, occurs moving heat from the cold to the hot side [22]. Most TEGs are built from two dissimilar semiconductor materials and two electrodes and are considered highly scalable, potentially highly efficient due to the lack of moving parts with no mechanical losses, and silent in operation [23]. These unique properties enable the utilization of small scale waste heat sources and the harvesting of abundantly available thermal energy which has been discussed in a large number of excellent reviews on thermoelectric materials [24], devices [21], and applications [21–23]. The potential of a TEG material to convert heat directly into electric energy is defined by the Seebeck coefficient $S_{Seebeck}$ [V/K] and is used to quantify the conversion efficiency of bulk thermoelectric compounds according to the zT figure of merit [25]:

$$zT = \frac{S_{Seebeck}{}^2 T}{\rho \kappa} \tag{3}$$

where T [K] is the average operating temperature, ρ [Ω.cm] the electrical resistivity and κ [W.m^{-1} K^{-1}] the thermal conductivity of the bulk thermoelectric material. The voltage V developed across the thermoelectric material assembly, with a given Seebeck coefficient and the available temperature difference ($T_{Cold} - T_{Hot}$) follows [19]:

$$V = \int_{T_{Cold}}^{T_{Hot}} S_1(T_{Hot}) - S_2(T_{Cold}) dT \tag{4}$$

for the Seebeck coefficient S_1 at the heat source temperature (T_{Hot}) and S_2 at the sink temperature (T_{Cold}). Based on the definition above, the maximum conversion efficiency η_{TE} of a TEG is limited by the Carnot efficiency and thus can be written as [26]:

$$\eta_{TE} = \frac{T_{Hot} - T_{Cold}}{T_{Hot}} \frac{\sqrt{1 + zT} - 1}{\sqrt{1 + zT} + \frac{T_{Cold}}{T_{Hot}}} \tag{5}$$

where the heat source temperature T_{Hot} and the figure of merit zT are the governing parameters. For a given heat source, the design of a TEG starts with the selection of the thermoelectric material. Ideally, a thermoelectric material is a poor thermal conductor but a good electrical conductor in order to obtain a high zT (Eq. (3)). Fig. 3 shows the thermoelectric zT figure of merit as a function of temperature for popular thermoelectric materials. The dotted lines refer to bulk materials and the solid lines refer to nanostructured materials. Fig. 3 also shows a very high dependence of zT as a function of temperature [24]. Since thermoelectric applications are temperature sensitive, the optimum properties of thermoelectric materials are limited to a narrow
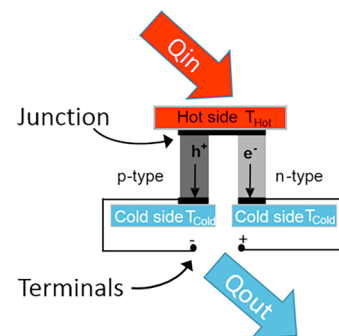

Fig. 2. Cross section schematic of a TEG module with a p-type semiconductor connected to an n-type semiconductor forming a junction at the hot side (T_{Hot}) and two electric terminals at the cold side (T_{Cold}).
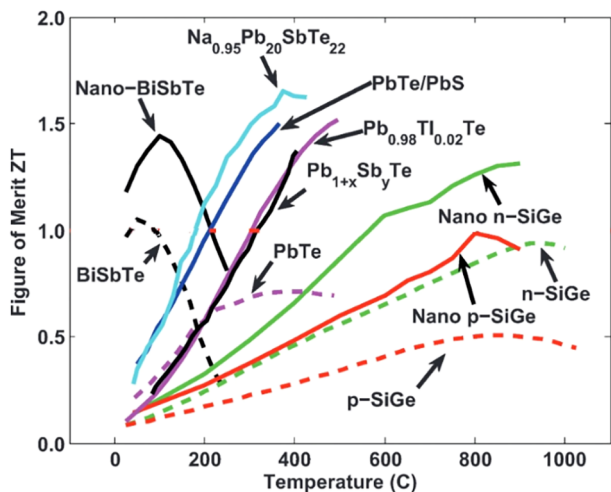
Fig. 3. Thermoelectric figure of merit zT as a function of temperature for thermoelectric materials. The solid lines refer to bulk materials. The dotted lines refer to nanostructured materials [24].

temperature window.

Amongst the most popular thermoelectric materials, for a heat source temperature between room temperature and 300 °C, are heavy metal alloys such as Bismuth (Bi), Tellurium (Te), Antimony (Sb) or Lead (Pb). Most commercially available thermoelectric modules are made of bulk Bismuth Telluride (Bi_2Te_3) semiconductors, designed to continuously operate at temperatures below 260 °C and intermittently at temperatures up to 380 °C. With an average zT of ~1 with $Bi_{0.4}Sb_{1.6}Te_3$ and SiGe, the assembled TEG modules provide reasonable power of 100 mW from temperature differences as small as 9 K [27]. Since the ideal operation temperature of bulk Bi_2Te_3 peaks at 100 °C, waste heat recovery and thermal energy harvesting is readily possible with Bi_2Te_3 modules with numerous commercial, industrial and scientific applications such as machine health monitoring with 80 μW/mm^2 at 100 °C (12 mW/150 mm^2) [28], automotive applications with 17000 μW/mm^2 at over 500 °C (500 W/28800 mm^2) [29], fuel cells with 150 μW/mm^2 (at 180 °C) [30,31], and wrist watches with 5.6 μW/mm^2 at 36 °C (22 μW/3.9 mm^2) [32]. However, the energy conversion efficiency of off-the-shelf modules with a zT of ~1 is well below 1%. Higher efficiencies with lead based thermoelectric modules are possible, where the zT peaks close to 1.5 at temperatures above 300 °C [24]. With heat source temperature above 300 °C, high heat fluxes are present and a need for water cooled or thin film TEGs arises in order to maintain continuous operation and a reasonable temperature difference

[33]. Maintaining a large temperature difference is needed to obtain a high efficiency, for which reason the optimization of bulk thermoelectric materials aims for a reduction of thermal conductivity to prevent energy loss from heat draining through the material. One approach suppressing thermal conductivity without a deterioration of electron transport, is to nano-engineer and geometrically optimize thin film thermoelectric materials [34]. Geometrical optimized films are 1 nm thick Bi_2Te_3/Sb_2Te_3 layers with a high zT of 2.4 at room temperature [35]. Other approaches utilize thermoelectric nano-wires [36] or band engineering strategies such as quantum dot super-lattices [37] in order to improve electrical conductivity and reduce thermal conductivity. These advanced TEG designs allow for an energy conversion efficiency between 1 and 2 % from a 20 K temperature difference (40 °C and 20 °C) delivering 0.04 μW/mm^2 [21]. Despite the reasonable efficiency of 1% near room temperature, there is also a need to extract the maximum power from the TEG. Since most thermoelectric applications are high current (~ 0.5A), but a relatively low voltage (< 0.3 V), methods such as impedance matching and application of DC-DC converters are needed to deliver stable voltages under varying temperature conditions [38,39]. In an effort to extend the range of TEG applications, ceramic-polymer composite thermoelectric materials have been developed. Composite TEGs enable transparent, flexible and stretchable applications with new possibilities for waste heat recovery and thermal energy harvesting, such as wearable electronics [40], bio-integrated systems and cybernetic applications [41].

Fig. 4 shows three types of wearable sensor nodes powered by a TEG energy harvester attached to various locations on the human skin. Composite TEGs are preferably made from a flexible material or manufactured on a flexible substrate, were they can be attached onto various locations of the skin with enhanced thermal contact on wrists (Fig. 4a) and arms (Fig. 4b + c). The graph for the wristband TEG in Fig. 4 shows an increasing power output with increasing thickness of the thermoelectric inorganic-polymer elements for varying polymer-thermoelectric filling factors F [42]. At an ambient temperature of 22 °C, the wrist TEG provides up to 350 μW of electric power, sufficient to drive wireless transceivers such as low power Bluetooth, ANT, or Zigbee. In order to increase the electric power in a TEG, the number of thermoelectric junctions can be simply increased by connecting TEGs in series, leading to a linear scaling. This linear behavior allows for a simplified design of TEG applications. The wide range of reliable and simple waste heat recovery and thermal energy harvesting applications with TEGs stems from this ability of modularization and the industrial scalability of the thermoelectric manufacturing process, and is further enabled by the discovery of new material synthesis and module TEG manufacturing techniques. Due to the simple TEG architecture it is easy to scale up or retrofit existing systems. For example, TEGs are best
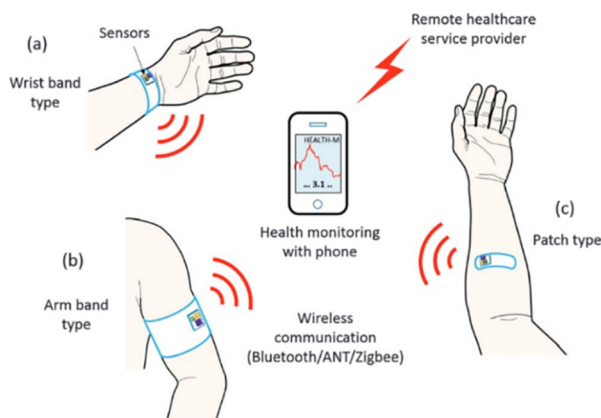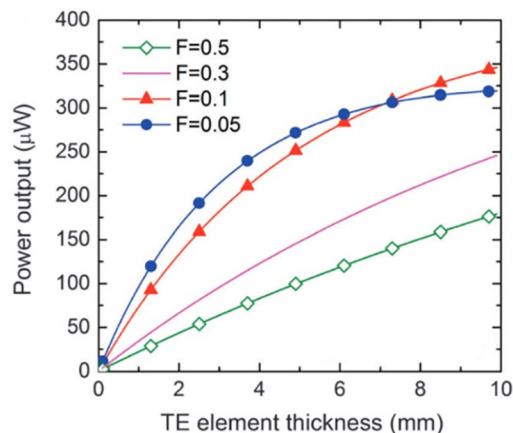

Fig. 4. Three types (a, b, c) of wearable sensor nodes powered by thermoelectric energy harvesters attached onto various locations of the skin with enhanced thermal contact for wireless data transmission to a smartphone [42].

utilized when the efficiency is less desirable than properties such as small size, low weight, or high reliability [20]. Traditional bulk devices are most appropriate for low heat flux systems [32] where efficiencies are limited to 2%, whereas composite TEGs are most suitable for wearable and flexible applications.

3. Thermionic converters

Thermionic energy converters (TIC), or thermionic generators, are solid state heat engines and therefore similarly to thermoelectric devices converting thermal energy directly into electrical energy. When a TIC is placed between a hot heat source and a cold heat sink, the hot electrode surface emits charge carriers (electrons). This charge emission process is based on the effect of thermionic emission, or the space charge effect, and enables a continuous surplus of electrons at the cold electrode which act as an electric power supply, continuously driving a direct electric current (DC) across an external load.

Fig. 5 shows a cross section schematic of a TIC with a hot emitter cathode (T_{Hot}) and a cold collector anode (T_{Cold}), separated by an inter-electrode gap d [m]. The inter-electrode gap exists as a vacuum, which allows for a thermionic electron emission process at the surface of the hot electrode. This effect is described by the electrode band theory and occurs when sufficient thermal energy is supplied to the TIC hot electrode in order to emit, or eject, electrons from the electrode surface into the vacuum space (similar to the photoelectric effect). The thermionic electron emission process is quantified by a work function (WF) for the electrode material. Only when an electron receives sufficient thermal energy from the emitter electrode, in excess of the Fermi level, can an electron cloud (or space charge accumulation) occur [43]. When the emitter electrode is maintained at a constant hot temperature, a continuous electron emission occurs from the hot electrode to the cold electrode in the TIC vacuum, leading to a surplus of charge at the cold receiver electrode. This surplus of charge translates into an electric potential difference across the generator terminals which can be discharged as a DC across an external electric load [44]. Recently, an excellent review on TICs for power generation was published [43]. In a TIC, the WF quantifies this electron emission and thermal energy transport process, and is defined as ϕ[eV] for the total current density J [A/cm^2] injected from the hot electrode to cold electrode [45]:

$$J = J_H - J_C = A_R A^* T_{Hot}^2 exp\left(-\frac{\phi_C + qV}{k_B T_{Hot}}\right) - A_R A^* T_{Cold}^2 exp\left(-\frac{q\phi_C}{k_B T_{Cold}}\right)$$

(6)

In Eq. (6), V is the voltage at the TIC terminals; J_H [A/cm^2] the current density injected from the hot electrode to the cold electrode and J_C the current density emitted from the cold electrode to hot electrode; q is the elementary charge [C], and k_B the Bolzman constant [46]. For the current density, the hot and cold electrode Richardson constant A_R [A/m^2 K^2] is for metals (120 A.m^{-2}.K^{-2}) and A^* for semiconductors, accounting for the doping concentration and electronic state density [47]. With TICs, the electron flow also carries heat from the hot side electrode to the cold side electrode, in conjunction with conventional thermal radiation, which contributes to the heat flow across the TIC generator. The heat carried by the electron flow from the hot to the cold electrode is expressed as Q'_e [W] [48,49]:

$$Q'_e = \frac{\partial Q}{\partial t} = J_H(2k_B T_{Hot} + q\phi_H + V) - J_C(2k_B T_{Cold} + q\phi_C + V)$$

(7)

which is linked to the output power density delivered and absorbed by the TIC, and the emissivity ε of the hot and cold electrode material ε_H and ε_C, respectively:

$$Q'_R = \sigma_{SB}(T_{Hot}^4 - T_{Cold}^4)(\varepsilon_H^{-1} - \varepsilon_C^{-1} - 1)^{-1}$$

(8)

which defines the power density delivered and absorbed. With the effective heat flow through the TIC, the thermionic generator efficiency

$\eta_{Thermionic}$ is defined as:

$$\eta_{Themionic} = \frac{P}{Q'_e + Q'_R}$$

(9)

where P [W] is the effective electric power output of the TIC. The theoretical efficiency of a TIC is only limited by the Carnot efficiency based on the available spatial temperatures difference between the two electrodes (Eq. (1)). A number of TICs utilizing heat induced thermionic emission have been theoretically and experimentally developed [43] along with the use of thermionic emission for refrigeration [50]. The governing parameter for the effectiveness of the TICs is the WF of the emitter electrode material and the corresponding temperature dependent energy barrier height $q\Phi$ (Eq. (6)).

Fig. 6 compares the maximum thermionic conversion efficiency for the electrode WF, and links the WF to the temperature of the hot electrode [51]. Most pure metal and semi-conductor electrodes have a high WF of over 3 eV and require heat source temperatures in excess of 720 °C in order to observe thermionic emission [58,59]. At high temperatures, over 15% conversion efficiency is possible with respective hot and cold electrode temperatures between 570 °C and 1300 °C, revealing that this technology is remarkably suitable for industrial and nuclear heat recovery applications [52,53,54]. Experimental devices show a high power density of 320 000 μW/mm^2 at temperatures in excess of 1000 °C [55]. However, with thermionic device the power density rapidly decreases at temperatures below 1000 °C, only generating 0.04 μW/mm^2 (9 nW/0.25 mm^2) at low temperatures [56]. When pure metal and semi-conductor electrodes are used in TICs, decreasing heat source temperatures lead to a diminishing electrode emission [50]. As shown in Fig. 6, the maximum conversion efficiency of a TIC with an electrode WF of 0.75 eV, at 127 °C hot electrode temperature and 27 °C cold electrode temperature, is close to 20%. In order to maintain the electron emission process at low temperatures, the corresponding electrode WF also needs to be low. Alkali metals and their oxides such as e.g. Lithium (Li), Potassium (K), and Cesium (Cs) have WFs lower than most metals and semiconductors, with typical values in the range between 2.1 eV and 2.49 eV [57] and their respective oxides between 0.4 eV and 1.8 eV [51,51a,59,60].

According to Table 1, Cesium Oxide (Cs$_2$O) coatings with a WF of 0.6 eV are potentially suitable for TICs operating at low temperatures [60]. However, the low WF usually implies an electrode melting point temperature close to room temperature. For this reason, the metal electrodes can be oxidized to form metal oxides in order to increase the melting point temperature and enable the operation of low WF electrodes. Theoretical approaches show that electrodes coated with alkali metal oxides in TICs can facilitate the ejection of electrons at near room temperature, and recover heat at temperatures as low as 27 °C [61]. In addition to the WF and the available temperature level, the efficiency of a TIC is also dependent on the inter-electrode gap distance d separating the hot emitter electrode from the cold electrode [62,63]. In this regard, Lee et al. determined the maximum efficiency adjusting the gap distance [56]. Since the radiative heat transfer is only in propagative mode, and independent of the gap distance, most TICs are micro-gap
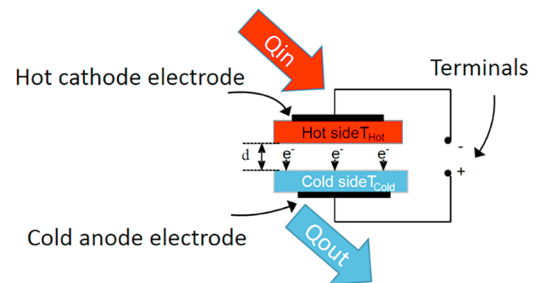

Fig. 5. Cross section schematic of a TIC with a hot (T$_{Hot}$) emitter cathode and a cold (T$_{Cold}$) receiver electrode, separated by an inter-electrode gap (d).
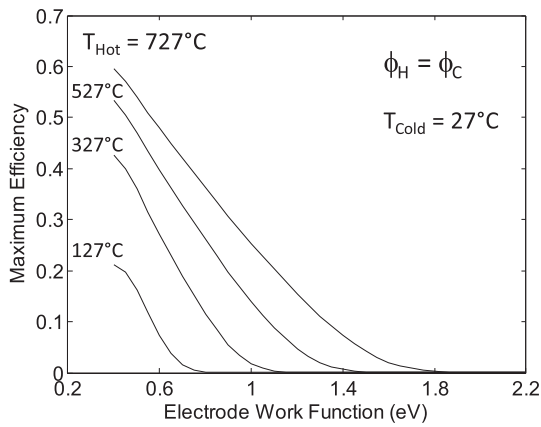
Fig. 6. Maximum thermionic conversion efficiency for the electrode work function (WF) dependent on the temperature of the hot electrode. The temperature of the cold electrode is maintained at 27 °C (modified from [51]).

Table 1
TIC emitter electrode materials and work functions (WF).

Material	Work function (eV)	Melting temperature (°C)	References
Si	4.85	1413	[58]
W	4.55	3421	[58]
LaB$_6$	2.60	2206	[47]
Li	2.49	180	[57]
BaO	2.30	1922	[47]
Cs	2.14	28	[58]
Cs$_2$O	0.60	490	[59]
K$_2$O$_2$	0.40	490	[60]

applications with high WFs [64–66]. However, an increase in electron injection is possible with gaps distances close to the thermal wavelength (wavelength = pulsation/speed of light). In the range of 5 nm to 100 nm, a significantly increase in electron injection level is possible due to tunneling effects, with up to six times higher currents compared to ordinary thermionic currents [62]. However, one of the main challenges with TICs is to maintain the high vacuum package with pressures between 10^{-3} and 10^{-9} mbar between the electrodes, which is needed for reliable and efficient applications. In addition, geometrical scaling issues with small gaps and large surfaces quickly arise. Therefore, the possibility of a solid-state thermionic generator with a solid contaminant layer has been proposed which helps to stabilize the device and support the gap between the electrodes [67]. At temperatures approaching room temperature, this type of solid-state thermionic power generator can be viewed as a bridge between vacuum-state thermionic convertors and thermoelectric power generators [68]. More recently, solid filled graphene electrode TIC heterostructures – without a vacuum gap – showed 7 to 8% efficiency from a waste heat temperature of 226 °C [69]. As an alternative to solid TICs, vapor or plasma filled gaps have been proposed which show unfavorably low efficiencies [70,62]. However, in practical applications it remains difficult to establish thermionic emission at low temperatures, due to the lack of low WF electrode materials. This insufficiency led to novel approaches like using photo excited thermionic emission, and the design of a photo excited thermionic generators. This new concept for utilizing solar energy for electricity generation and photon-enhanced thermionic emission combines quantum and thermal-mechanisms into a single physical process [71]. This combined energy converter operates at 50% overall efficiency. However, like thermoelectric devices, thermionic systems are considered a low voltage application, since the electrode band gap is low [72]. In contrast, the ease of a serial or parallel connectivity enables greater scaling possibilities, compared to other types of generator applications. The downside with TICs is the need for high heat source temperatures. However, with low WF electrodes, low

temperature waste heat recovery becomes possible. For this reason, thermionic devices are considered comparable, or even superior, to thermoelectric modules, because they maintain a gap between the hot and cold source, minimizing thermal losses.

4. Pyroelectric harvesters

Pyroelectric generators, or pyroelectric energy harvesters, are solid state heat engines and convert thermal energy directly into electrical energy. In a pyroelectric harvester every change in temperature translates into an electric potential difference across the generator terminals. This potential difference is based on the pyroelectric effect, which describes the change in the crystallographic polarization moment of a pyroelectric material, in response to the change in temperature ΔT [73]. For cyclic, or time variant (Δt), heating and cooling ($\Delta T/\Delta t$) the pyroelectric energy harvester generates an alternating current (AC) across the generator terminals proportional to experienced change in temperature. In this way, pyroelectric energy harvesters are different from the previously discussed thermoelectric generators and thermionic converters where the current is proportional to the spatial temperature gradient.

Fig. 7 shows a cross section schematic of a hot and cold pyroelectric harvester element with a top and bottom electrode. The cold pyroelectric material exhibits a spontaneous polarization $P_{Polarization}$ [C/m^2] moment, or remnant polarization moment, perpendicular to the electrode surface area. When the pyroelectric material is heated Qin (dt) or cooled Qout (dt) over time, the spontaneous polarization moment changes ($\Delta P_{Polarization}$). Based on electrostatic principles, the change in spontaneous polarization moment perpendicular to the electrodes surface causes surface bound charge at the pyroelectric material-electrode interface to be repelled or attracted [74]. When the surface bound charge is repelled, free electrons are available as electric potential difference, or voltage V, across the two electrode terminals. The potential difference V in a pyroelectric harvester is dependent on the pyroelectric material and the change in temperature ΔT, and can be discharged as an electric current across an external electric load. The converse pyroelectric effect is known as the electrocaloric effect, in which heat is pumped into the system when an external electric field is applied. Most pyroelectric and electrocaloric applications are limited to temperatures below the Curie temperature T_c [K], where the materials lose their spontaneous polarization moment [75]. The ability of a pyroelectric material to transform a change in temperature (ΔT) into a change in polarization ($\Delta P_{Polarization}$) is quantified by the pyroelectric coefficient $p*$:

$$p^* = \frac{\Delta P_{Polarization}}{\Delta T} \tag{10}$$

The effective change in polarization ($\Delta P_{Polarization}$) can be directly measured as a short circuit pyroelectric current I [A] [74]:

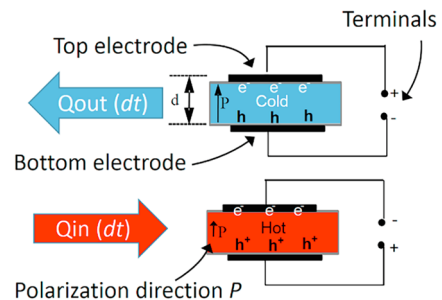$$I = p^* A \frac{\Delta T}{\Delta t} \tag{11}$$

Fig. 7. Cross section schematic of a cold (top) and a hot (bottom) pyroelectric harvester.

or as an open circuit voltage V [V]:

$$V = \frac{p^*}{\varepsilon} d. \, \Delta T \tag{12}$$

at the harvester terminals, with the electrode surface area A [m^2], effective permittivity ε [F/m], and electrode distance d [m]. Assuming a parallel plate capacitor geometry for the pyroelectric device structure in Fig. 7, the available potential difference and the electrical energy E [J] density stored in the pyroelectric element ($E = \frac{1}{2} C.V^2$) translates to [75]:

$$E = \frac{1}{2} \frac{p^{*2}}{\varepsilon} A. \, d. \, \Delta T^2 \tag{13}$$

for the given geometrical dimensions (electrode distance d and electrode surface area A). With the available energy E, the pyroelectric energy harvester efficiency $\eta_{Pyroelectric}$ is defined as [76]:

$$\eta_{Pyroelectric} = \frac{E}{Q} \tag{14}$$

for the transferred heat load Q [J]. Since pyroelectric harvesters convert thermal energy from heating and cooling into electricity, the theoretical conversion efficiency is close to 50% of the Carnot efficiency [76,10]. Most pyroelectric materials are polar dielectric materials and belong to the subclass of ferroelectrics. Ferroelectric materials are single crystal, polycrystalline ceramic or crystal polymer materials. All pyroelectric materials also exhibit piezoelectric activity which can be utilized for mechanical energy generation and energy harvesting [77]. According to Eq. (13), a high energy yield is given for a pyroelectric material with a high pyroelectric coefficient p^* and a low permittivity ε [78]. In order to determine a pyroelectric materials based on their ability to produce electricity from heat, the pyroelectric coefficient p^* and the permittivity can be express in a pyroelectric figure of merit F_E:

$$F_E = \frac{p^{*2}}{\varepsilon} \tag{15}$$

Fig. 8 compares the F_E against the heat capacity of pyroelectric materials. The heat capacity must be low in order to experience a large change in temperature ΔT for the available heat load Q, and effectively convert heat into electricity (Eq. (11)). A large number of pyroelectric materials are thoroughly reviewed [79,80] as well as pyroelectric materials in the context of energy harvesting [75].

According to Fig. 8, amongst the most powerful materials, with a pyroelectric coefficient of $p^* = 1790 \, \mu C/m^2 \, K$, is a single crystal lead (Pb) magnesium (Mg), niobate (Nb) – lead (Pb) titanate (Ti) – PMN-0.25PT which has a pyroelectric figure of merit F_E above 100 [75]. However, due to the low Curie phase transition temperature of 120 °C, PMN-0.25PT is limited to low temperature pyroelectric energy harvesting applications. Most materials with a higher curie temperature of 180 °C belong to the group of lead (Pb) zirconate (Zr) titanate (Ti) oxides – PbZr$_x$Ti$_{1-x}$O$_3$. Due to the reasonable pyroelectric coefficient of $p^* = 400 \, \mu C/m^2 \, K$, PZT is readily used for pyroelectric energy harvesting applications [81]. Concerning lead free pyroelectric materials Triglycine Selenate (TGS) has a high pyroelectric coefficient of 420 $\mu C/m^2 \, K$ [82] as well as Strontium (Sr), Barium (Ba) and Niobium (Nb) – Sr$_{0.5}$Ba$_{0.5}$Nb$_2$O$_6$ (SBN) with a pyroelectric coefficient of $p^* = 650 \, \mu C/m^2 \, K$ [83]. In some pyroelectric applications the pyroelectric materials are substrate mounted films [84], but mostly pyroelectric harvesters are free standing generators. In an effort to improve energy harvesterssting capabilities, geometrical optimization using nano-manufacturing technologies were developed to enables the design of Zinc oxide (ZnO) nanowire pyroelectric harvesters, which show pyroelectric and thermoelectric activity [85]. Another lead free pyroelectric material suitable for energy harvesting applications is Polyvilylidene Difluoride (PVDF). PVDF is, compared to ceramics, a pyroelectric active polymer with a pyroelectric coefficient of $p^* = 25 \, \mu C/m^2 \, K$ [86]. In contrast to ceramics, PVDF polymers have unique mechanical properties of high

tensile stress and low weight. With flexible PVDF, or more powerful PVDF derivative PVDF-TrFe films, low cost pyroelectric energy harvesters can be simply attached to an external resistor [87]. However, due to the AC nature of pyroelectric harvesters, AC to DC rectification is needed for most applications [88]. The fact that pyroelectric generators supply AC stems from the temperature variations or alternating heat flows needed for thermal energy conversion. When the pyroelectric harvester is optimized for externally induced temperature variations, pyroelectric generators can exceed a 40 V terminal voltage and micro amperes of electric current [86], for which reason most pyroelectric energy harvesters are considered high voltage and low current application. In practical applications passive pyroelectric generators utilize slow, small and rare natural temperature changes. Successful harvesting applications have been demonstrated for road vibrations [89] and thermal impacts [90], harvesting mechanical and thermal energy. At room temperature, natural temperature fluctuations were harvested with PVDF. However, since natural day and night temperature fluctuations are small and slow, the peak voltage was just 2 V delivering only 0.004 $\mu W/mm^2$ of electric power [91]. Certain weather conditions allow for pyroelectric solar radiation energy harvesting, due to the shade produced by passing clouds, and deliver 0.01 $\mu W/mm^2$ (4.9 $\mu W/$ 500 mm^2) [92]. However, the utilization of natural and slow temperature oscillations creates a necessity for energy storage circuits with pyroelectrics [93]. Efforts to increase the temperature variation frequency and the temperature gradient include a self-induced pyroelectric heat engine which makes use of a bi-stables membrane for mechanical temperature switching. The conversion of thermal to mechanical energy then generates an open circuit voltage of up to 13 V (primarily utilizing the piezoelectric effect) and delivers 0.03 $\mu W/mm^2$ at an efficiency of 1.2×10^{-6}% [94]. These active types of generators require external control units which are considered a parasitic loss for the harvester. A more advanced approach of pyroelectric energy harvesting is to modulate the level of polarization $P_{Polarization}$ of the pyroelectric material by applying an external electrical field while changing the temperature ΔT. With the external electric field, the polarization and the change in temperature is constantly maintained until enough electric charge is stored in the pyroelectric harvester. This controlled operation principle of a pyroelectric harvester is known as a thermodynamic Olsen cycle [95]. With the Olsen cycles, significant improvements in the power density (6.5 $\mu W/mm^2$) and efficiency 1.3% of PMN-PT were achieved [96]. Recently, a laser modulated Olsen cycles reported an extremely high energy density of up to 40 $\mu W/mm^2$ using
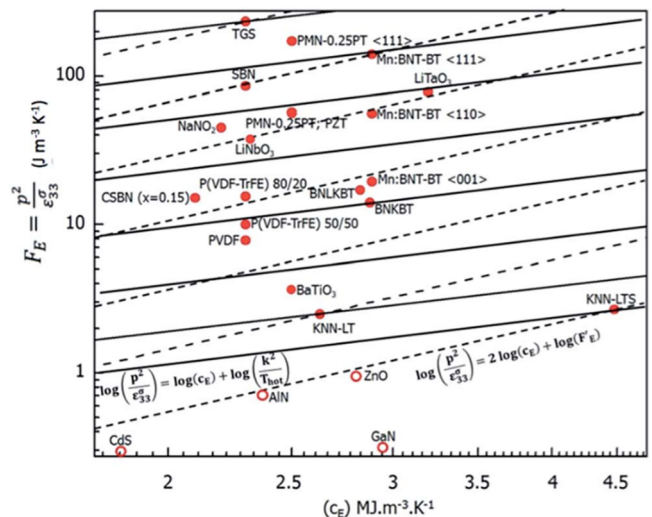

Fig. 8. The pyroelectric figure of merit for different materials in an Ashby diagram expressing the pyroelectric coefficient and permittivity. Ferroelectric materials are indicated by solid circles and non-ferroelectric materials by open-circles [75].

sophisticated device manufacturing and Olsen circuit control techniques [97]. The Olsen cycle was also successfully utilized in a pyro-electric generator using liquid-based switchable thermal interfaces [98].

According to Fig. 9, the liquid switchable interfaces enables a transition between the conductive and non-conductive liquid state which is synchronized with the external electrical polarization field. Cycling heat between a heat source and a heat sink provides remarkably high power densities of up to 7 μW/mm² from a temperature difference of 80 K. Similar theoretical designs employ a cantilever structure which mechanically switches the heat flow using bimetals (such as those used in thermostats) which operate between a spatial temperature gradient and convert heat into the temperature fluctuation needed for pyro-electrics energy harvesting [99]. Since all pyroelectric materials are also piezoelectric, hybrid mechanical and thermal type generators are possible and proved to be very powerful [100]. Here, the harvester experiences mechanical motion and introduced piezoelectric activity in the pyroelectric harvester materials [101]. More recently, a novel type of pyroelectric energy harvester was developed using an oscillating heat pipe-pyroelectric assembly and continuously generates electrical energy from a spatial heat gradient. The pyroelectric elements absorb heat from an evaporating and condensing fluid in a oscillating heat pipe and recover high thermal loads between 60 °C and 25 °C with an effective change in temperature of 5 K. This allows an external 50 pF storage capacitor to be charged to 0.2 V within 50 s [102]. Certain environmental circumstances also allow for mechanical and thermal energy to be simultaneously explored. A wind driven pyroelectric generator utilizes a wind induced rapid changes in temperature when the sun is shining and the wind is strong [103]. The future of pyroelectric energy harvesting lies in small generator thermal masses which allow for rapid and high changes in temperature. On the other hand, the AC nature of pyroelectric harvesters requires rectification and power conditioning which leads to transformation losses. With the need for temperature oscillation and the relatively low Curie temperature, pyroelectric energy harvesters remain a low temperature application. The possibility of harvesting both mechanical energy using the piezoelectric effect and thermal energy using the pyroelectric effect, provides a challenging opportunity for future energy harvesting with pyroelectric materials.

5. Thermomagnetic generators

Thermomagnetic generators, or thermo-magneto-electric generators, are solid state heat engines and convert thermal energy directly into electrical energy. In a thermomagnetic generator every change in temperature (ΔT) translates into an electric current across the generator terminals. When heated, the ferromagnetic material in the thermomagnetic generator experiences a crystallographic phase transition
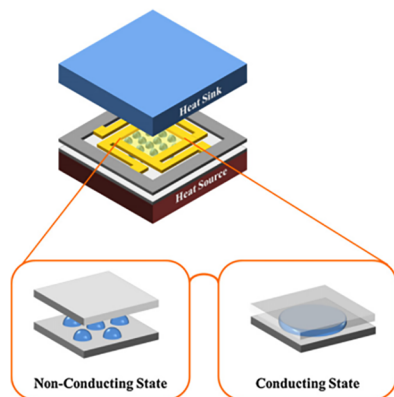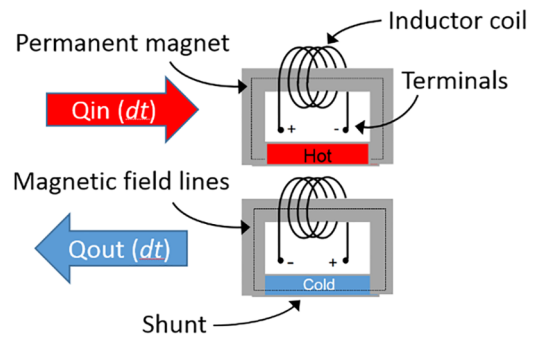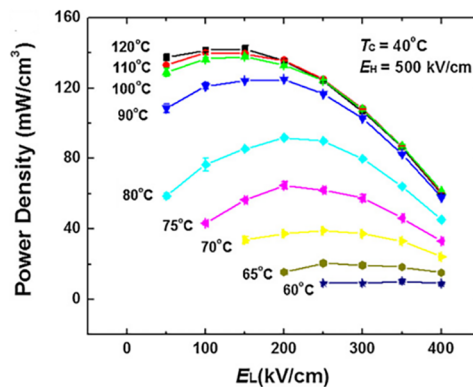

Fig. 10. Cross section schematic of a hot thermomagnetic generator (top) and a cold thermomagnetic generators (bottom) with a ferromagnetic shunt clamped across a C-shaped permanent magnet.

followed by a rapid change in the magnetic moment. This change in magnetic moment induces an electromagnetic induction force (EMF), or electromotive force, and drives an electric current across an external electric load. For cyclic, or time variant (Δt), heating and cooling ($\Delta T/\Delta t$) the thermomagnetic generator drives an alternating current (AC) across the generator terminals proportional to the experienced change in temperature.

Fig. 10 shows a cross section schematic of a solid-state thermomagnetic generator which consists of an electrical inductor coil wound around a C-shaped external hard permanent magnet with a soft ferromagnetic material placed between the two poles as a shunt. The ferromagnetic shunt has a temperature sensitive magnetic permeability and guides the magnetic field lines of the permanent magnet. When the shunt is heated over time by Qin (dt) through the phase transition temperature, or Curie temperature (T_c), the permeability of the shunt changes which consequently alters the intensity of the magnetic flux through the C-shaped permanent magnet [104]. Every change in magnetic flux of the C-shaped permanent magnet then induces an electric current in the inductor coil, which is available as electric power across the generator terminals and described by Faraday's law. When the shunt material is cooled, the magnetic field in the external permanent magnet restores and induces a reverse electrical current in the inductor coil. If the ferromagnetic shunt is sequentially heated and cooled, the thermomagnetic generator drives an alternating current (AC) across the generator terminals [105]. The induced voltage V in the thermomagnetic generator as in Fig. 10 is defined as [106]:

$$V = -NS\frac{dB}{dt} \tag{16}$$

where N is the number of turns in the inductor coil, S [m²] is the

Fig. 9. Pyroelectric energy harvesting using liquid-based switchable thermal interfaces [98].

average area enclosed by the inductor coil and dB [T] is the change in magnetic flux. The change in magnetic flux dB divided by the change in time dt is then defined as [106,107]:

$$\frac{dB}{dt} = \frac{\left(H - \frac{B}{\mu_s \mu_o}\right) R}{n_0^2 L_s S} \qquad (17)$$

where L_s is the shunt length, μ_s is the relative permeability of the shunt and μ_0 the vacuum permeability [H/m], n_o [m^{-1}] is the turns per unit length of the inductor coil, R the coil resistance [Ω] and H the total magnetic field [A/m]. The temperature sensitive permeability of the shunt material and the corresponding rate of change in permeability determines the efficiency of the thermomagnetic generator to convert heat into electricity. The temperature dependent change in permeability of the shunt is modelled as [106]:

$$\mu_s = \mu_C + A_C (T_c - T)^x \qquad (18)$$

where μ_c is the relative permeability of the Curie point, T_c the Curie temperature and T the shunt temperature. A_C and X are empirical derived constants. For a given change in the temperature ΔT of the shunt material, the efficiency of a thermomagnetic generator is identified as [108]:

$$\eta_{Thermomagnetic} = \frac{\pi}{4\sqrt{2}} \frac{\Delta T}{T_c} \qquad (19)$$

assuming the change in temperature ΔT crosses the Curie temperature T_c of the shunt material (for an effective change in permeability). If heat is supplied and removed periodically to the ferromagnetic shunt, the temperature range should ideally remain within a very narrow temperature window, just above and below T_c. Consequently, this type of thermomagnetic generator has the potential to work at very high efficiencies when utilized for heating and cooling, due to the lack of mechanical motion. A number of excellent reviews on thermomagnetic materials [109] and devices [104] are available. Efficiency estimates report between 55% and 75% of the theoretical Carnot efficiency [109]. The key component of the thermomagnetic generator is the ferromagnetic shunt material. Ferromagnetic materials usually have a high Curie temperature, such as ferromagnetic Iron (Ir) which shows a large drop in the magnetic moment at the Curie phase transition temperature of over 700 °C [104], as well as other ferromagnetic materials such as Cobalt ($T_c = 1120$ °C) or Nickel ($T_c = 358$ °C). For waste heat recovery and thermal energy harvesting applications, the ideal ferromagnetic shunt material should have a phase transition temperature below the heat source temperature. Soft ferromagnetic materials e.g. nickel alloys usually have a lower T_c. The first practical thermomagnetic generator employed Gadolinium (Gd) with a low transition temperature of 16.85 °C (Gd) [108]. It was experimentally demonstrated to recover low

temperature heat utilizing the phase transition of ferromagnetic Gd single crystals at room temperature [110]. Following the successful utilization of a transition temperature close to room temperature, a number of Gd-shunt thermomagnetic generators have been theoretically proven to produce up to 0.8 μW/mm² (318 μW/400 mm²) [111] at an efficiency between 0.13% and 0.8% [112,113]. Other shunt materials, with a sudden transition from ferromagnetic to paramagnetic moment and a transition temperature of 167 °C, are Nickel (Ni), Cobalt (Co), Magnesium (Mn) and Tin (Sn) alloys – Ni$_{45}$Co$_5$Mn$_{40}$Sn$_{10}$, also referred to as Heusler alloys. Experimental Heusler thermomagnetic generators demonstrated a voltage of 0.7 V (AC) across an external 10 kΩ resistor from a temperature window of 10 K, which translates into 50 μW for a disc shape generator with a diameter of 7.5 mm (1.1 μW/mm²) of electrical power at an efficiency of 0.004% [114]. In the Heusler thermomagnetic generator, the magnetic field goes through a particular strong aluminum, nickel- and cobalt-alloy (AlNiCo) counterpart. A similar AlNiCo alloy was used in a Tungsten thermomagnetic generator which showed an efficiency of 2% from temperature differences as low as 6 K [104]. This concept was further developed with Ni$_{44}$, Co$_6$, Mn$_{40}$, and Sn$_{10}$ at a phase transition temperature of 126 °C [115]. Among the materials with the largest change in magnetic permeability is Holmium (Ho), with a ferromagnetic to antiferromagnetic phase transition [116]. However, the phase transition temperature with Ho is 20 K and too low for any practical generator and energy harvesting applications. Despite the limited number of shunt materials available and the need for cycling temperature changes, various conceptual thermomagnetic generator designs exist. One generator design uses an external heat sources at a temperature ranging from 90 °C to 225 °C in order to experimentally demonstrate thermomagnetic energy generation from a continuously alternating hot and cold fluid reservoir [107]. A similar experimental approach uses a manually controlled water valve to cycle heat from external tanks in a thermomagnetic generator [117]. However, for standalone thermomagnetic generators a self-induced temperature cycling technique is needed in order to continuously generate electricity from heat.

Fig. 11(a) shows a thermomagnetic generator which mechanically switches the ferromagnetic shunt temperature. This mechanic-thermomagnetic generator uses a soft ferromagnetic material suspended on a serpentine spring near a permanent magnetic material [105]. The principle of the device relies on the thermally induced second order phase transition producing mechanical energy, which is subsequently converted to electrical energy. The spatial temperature difference between the hot side, maintained at 50 °C, and the cold side, maintained at 0 °C, produced 35 μW/mm² of electric power for a hot/cold gap distance of 0.2 mm. A similar mechanical-thermomagnetic assembly employed a thermomagnetic restoring spring mechanism, and converted mechanical energy into electrical energy using the piezoelectric
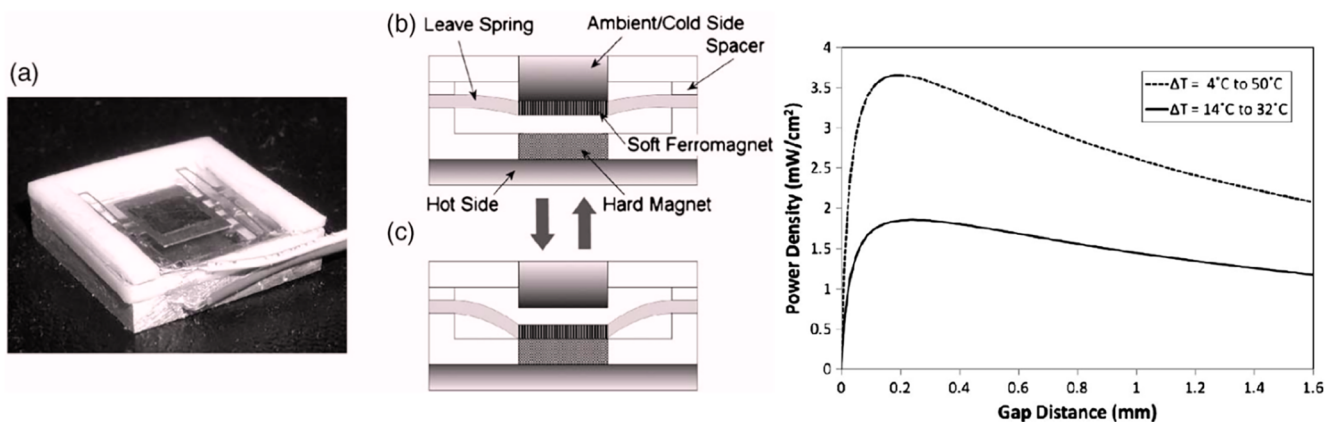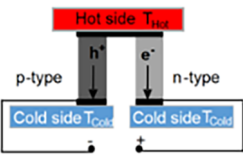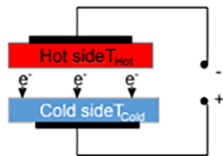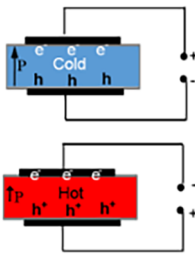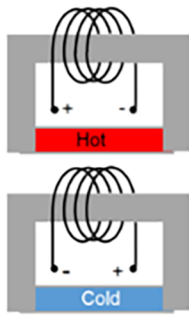

Fig. 11. Schematic diagram of a thermomagnetic generator (a) with a leaver spring (b) cycling heat (c) between a hot heat source and a cold heat sink distance and the corresponding power density of the generator [105].

Table 2
Solid state thermal generators and energy harvesters.

Comparison	Thermoelectric generator	Thermionic converter	Pyroelectric harvester	Thermomagnetic generator
Architecture				
Heat transfer mode	Spatial temperature gradient (ΔT)	Spatial temperature gradient (ΔT)	Transient change in temperature ($\Delta T/\Delta t$)	Transient change in temperature ($\Delta T/\Delta t$)
Temperature range [°C]	35–1000	180–1700	20–200	10–1120
Material	Semiconductors compounds: e.g. Bi_2Te_3, SiGe	Semiconductor compounds: e.g. Cs_2O/Si, K_2O_2/Si	Crystalline ceramics and polymers: e.g. $BaTiO_3$, $LiNbO_3$, PVDF	Ferromagnetic metals, alloys, oxides: e.g. Co, Fe, Ni, Mn
Electron transport mechanism	Drift diffusion	Thermionic electron emission	Coulomb forces	Electromagnetic induction
Type of thermal losses	Thermal conduction	Thermal radiation	Thermal diffusion	Thermal diffusion
Theoretical 1st law efficiency ($T_{Cold} = 27$ °C and $T_{Hot} = 128$ °C)	5% with zT = 1 (Bi_2Te_3)	20% with $\varnothing = 0.4$ eV (K_2O_2)	12.5%	19%
Experimental efficiency [%]	0.1–2	0.09–14.7	< 1.3	0.166–2
Energy density [$\mu W/mm^2$]	0.04–17 000	0.04–324 000	0.004–40	0.16–35
Output current	DC	DC	AC	AC

effect [118]. This design developed high voltages between 5 and 50 V due to the high potential open circuit voltages possible with piezoelectric devices. The concept of combining thermomagnetic and piezoelectric principles was extended to thermomagnetic actuated piezoelectric-pyroelectric cantilever systems, exchanging the heat flow between the hot source and cold sink [119]. Apart from the changes in permeability with the thermomagnetic shunt, mechanical forces also change the geometry of the shunt. This mechanical component also leads to a subclass of thermomagnetic heat engines utilizing magnetostriction effects. Magnetostrictive thermomagnetic devices, thermomagnetic mechanical heat engines or Curie motors, are designed to convert heat into mechanical motion and subsequently into electrical energy [113]. Compared to natural temperature oscillations, these experimental thermomagnetic generators shows a relatively high alternating frequency of 1.56 Hz, and an AC peak voltage between 1.5 and 2.2 V. Other forms of cantilever designs include a mechanical Cu-Zn cantilever beam, converting thermal energy into mechanical energy and subsequently into electrical energy [120]. When close to the resonance frequency, the thermo-mechanical-electrical system receives thermal energy at 160 °C and provides up to 0.16 $\mu W/mm^2$ (2.4 $\mu W/$ 15 mm^2) of electric power. However, heat cycling and rectification/power-conditioning the AC output power is required for most applications, due to the low voltage nature. Furthermore, since most thermomagnetic materials are metals, generator weight is relatively high. Interesting opportunities for dense generator packages exist as the thermal conductivity and the mechanical expansion of the shunt allows for the development of an active thermomagnetic device with strong changes in the magnetic field. For this reason, thermomagnetic generators remain at an early experimental stage and therefore have not yet been commercially exploited.

6. Conclusions

The conversion of low temperature heat into electrical energy has been exploited by numerous technologies and has many applications

available. Solid-state heat engines, thermal to electrical energy converters and energy harvesters are standalone generators, which allow for local powering of small-scale electronic devices as well as autonomous and self-sustainable applications, without the need for maintenance and additional costs. Table 2 shows a summary of the key design parameters for thermoelectric generators, thermionic converters, pyroelectric harvesters and thermomagnetic generators.

The main key design parameter for the generators and energy harvesters in Table 2 is the heat transfer mode. With thermoelectric and thermionic devices a spatial temperature gradient is needed compared to the transient change in temperature with pyroelectric and thermomagnetic devices. For the same reason, thermoelectric and thermionic converters supply a direct current (DC) which is desirable for most modern electronics and for electrical energy storage. In particular, thermoelectric modules show recent material engineering efforts which have improved the power output by 50% under laboratory conditions, when compared to off-the-shelf BiTe modules. With scalable and flexible thermoelectric modules, it becomes possible to extend the field of application into wearable devices and operation under harsh conditions. With respect to the heat source temperature, technically viable thermoelectric waste heat recovery technologies need a heat source temperature of 100 °C which shows reasonable generator power densities of up to 80 $\mu W/mm^2$. On the other hand, thermionic converters require a relatively high heat source temperature, well above 100 °C, in order to deliver a direct current. Highly efficient electrode coatings exist but require further material engineering efforts in order to maintain durability. Currently, there are no real world applications at temperature below 100 °C available. However, the intrinsic feature of low thermal conductivity and the potentially high efficiency of 20% might enable powerful waste heat recovery and thermal energy harvesting applications in the future using advanced electrode materials. Compared to the spatial temperature gradients required by thermoelectric and thermionic devices, pyroelectric and thermomagnetic devices requires a transient change in temperature. For this reason, pyroelectric energy harvesting applications are restricted to a low heat

exchange because the pyroelectric material is a thermal and electrical insulator. From a material point of view, pyroelectric harvesters can be very thin and are highly flexible, and work well for temperature oscillations. Due to the simple architecture, pyroelectric energy harvesters and thermionic devices can be easily fabricated using sophisticated device manufacturing and material deposition techniques, and have a high potential to deliver promising energy harvesting applications. Similar to pyroelectrics harvesters, thermomagnetic generators also need a transient, or oscillating, change in temperature. Since most thermomagnetic materials are metals, rapid temperature fluctuations are possible. For this reason, thermomagnetic generators show a high power density of up to $35\,\mu W/mm^2$ when converting thermal energy into electrical energy at a temperature of $50\,°C$. However, the inconvenient exchange of heat leads to a lack of waste heat recovery possibilities with only a small number of experimental thermomagnetic solid state applications. In general, most solid state heat engines for waste heat recovery and thermal energy harvesting show a potentially high energy conversion efficiency, but remain a low power application. Since the temperature level is usually not adjustable in waste heat recovery and thermal energy harvesting, every technology has to be tailored to the heat source. From an economical point of view the engineering efforts needed to design a device and the costs of the materials remain high, for which reason the right spectrum for applications needs to be found.

Conflict of interest

The authors declared no conflicts of interest.

Acknowledgements

References

[1] IRENA. REthinking Energy 2017, 2017 at http://www.irena.org/-/media/Files/IRENA/Agency/Publication/2017/IRENA_REthinking_Energy_2017.pdf.

[2] B.F. Tchanche, G. Lambrinos, A. Frangoudakis, G. Papadakis, Low-grade heat conversion into power using organic Rankine cycles – a review of various applications, Renew. Sustain. Energy Rev. 15 (2011) 3963–3979, https://doi.org/10.1016/j.rser.2011.07.024.

[3] K. Ebrahimi, G.F. Jones, A.S. Fleischer, A review of data center cooling technology, operating conditions and the corresponding low-grade waste heat recovery opportunities, Renew. Sustain. Energy Rev. 31 (2014) 622–638, https://doi.org/10.1016/j.rser.2013.12.007.

[4] L.E. Bell, Cooling, heating, generating power, and recovering waste heat with thermoelectric systems, Science (80-.) 321 (2008) 1457, https://doi.org/10.1126/science.1158899 LP-1461.

[5] S. Boisseau, G. Despesse, B. Ahmed. in Small-Scale Energy Harvesting, 2012. https://doi.org/10.5772/51360.

[6] Energy, U. S. D. of. Waste Heat Recovery: Technology and Opportunities in U.S. Industry. 2008.

[7] A. Landelle, N. Tauveron, P. Haberschill, R. Revellin, S. Colasson, Organic Rankine cycle design and performance comparison based on experimental database, Appl. Energy 204 (2017) 1172–1187, https://doi.org/10.1016/j.apenergy.2017.04.012.

[8] W.K.G. Seah, A.E. Zhi, H.P. Tan, Wireless sensor networks powered by ambient energy harvesting (WSN-HEAP) – survey and challenges, in: Proceedings of the 2009 1st International Conference on Wireless Communication, Vehicular Technology, Information Theory and Aerospace and Electronic Systems Technology, Wireless VITAE 2009, 2009. https://doi.org/10.1109/WIRELESSVITAE.2009.5172411.

[9] O. Jeong, S. Konishi, Fabrication and drive test of pneumatic PDMS micro pump, Sensors Actuators A. Phys. 135 (2) (2007) 849–856, https://doi.org/10.1016/j.sna.2006.09.012.

[10] G. Sebald, E. Lefeuvre, D. Guyomar, Pyroelectric energy conversion: optimization principles, IEEE Trans. Ultrason. Ferroelectr. Freq. Control 55 (3) (2008) 538–551, https://doi.org/10.1109/TUFFC.2008.680.

[11] J. Henkel, S. Pagani, H. Amrouch, L. Bauer, F. Samie, Ultra-low power and dependability for IoT devices (Invited paper for IoT technologies), in: Proceedings of the 2017 Design, Automation and Test in Europe, DATE 2017, 2017. https://doi.org/10.23919/DATE.2017.7927129.

[12] Kishore, Ravi Anant, S. Priya, A review on low-grade thermal energy harvesting: materials, methods and devices, Materials (Basel) 11 (2018) 1433, https://doi.org/10.3390/ma11081433.

[13] J. Roßnagel, S.T. Dawkins, K.N. Tolazzi, O. Abah, E. Lutz, F. Schmidt-Kaler, K. Singer, A single-atom heat engine, Science (80-) 352 (6283) (2016) 325–329, https://doi.org/10.1126/science.aad6320.

[14] A.L. Cottrill, A.T. Liu, Y. Kunai, V.B. Koman, A. Kaplan, S.G. Mahajan, P. Liu, A.R. Toland, M.S. Strano, Ultra-high thermal effusivity materials for resonant ambient thermal energy harvesting, Nat. Commun. 9 (1) (2018) 664, https://doi.org/10.1038/s41467-018-03029-x.

[15] B. Sothmann, M. Büttiker, Magnon-driven quantum-dot heat engine, EPL (2012), https://doi.org/10.1209/0295-5075/99/27001.

[16] T.I. Quickenden, A review of power generation in aqueous thermogalvanic cells, J. Electrochem. Soc. (1995), https://doi.org/10.1149/1.2048446.

[17] S.Y. Wu, L. Xiao, Y.D. Cao, A review on advances in alkali metal thermal to electric converters (AMTECs), Int. J. Energy Res. (2009), https://doi.org/10.1002/er.1584.

[18] F.P. Incropera, D.P. DeWitt, T.L. Bergman, A.S. Lavine, Fundamentals of heat and mass transfer, Water (2007), https://doi.org/10.1016/j.applthermaleng.2011.03.022.

[19] S. Percey, C. Knight, S. McGarry, A. Post, T. Moore, K. Cavanagh, Thermal energy harvesting for application at MEMS scale, Springer, 2014, https://doi.org/10.1007/978-1-4614-9215-3.

[20] F.J. DiSalvo, Thermoelectric cooling and power generation, Science (80-.) (1999), https://doi.org/10.1126/science.285.5428.703.

[21] W. He, G. Zhang, X. Zhang, J. Ji, G. Li, X. Zhao, Recent development and application of thermoelectric generator and cooler, Appl. Energy (2015), https://doi.org/10.1016/j.apenergy.2014.12.075.

[22] X. Zhang, L.-D. Zhao, Thermoelectric materials: energy conversion between heat and electricity, J. Mater. (2015), https://doi.org/10.1016/j.jmat.2015.01.001.

[23] S.B. Riffat, X. Ma, Thermoelectrics: a review of present and potential applications, Appl. Therm. Eng. (2003), https://doi.org/10.1016/S1359-4311(03)00012-7.

[24] A.J. Minnich, M.S. Dresselhaus, Z.F. Ren, G. Chen, Bulk nanostructured thermoelectric materials: current research and future prospects, Energy Environ. Sci. (2009), https://doi.org/10.1039/b822664b.

[25] J.R. Szczech, J.M. Higgins, S. Jin, Enhancement of the thermoelectric properties in nanoscale and nanostructured materials, J. Mater. Chem. (2011), https://doi.org/10.1039/c0jm02755c.

[26] C. Goupil, W. Seifert, K. Zabrocki, E. Müller, G.J. Snyder, Thermodynamics of thermoelectric phenomena and applications, Entropy (2011), https://doi.org/10.3390/e13081481.

[27] R. Venkatasubramanian, C. Watkins, D. Stokes, J. Posthill, C. Caylor, Energy harvesting for electronics with thermoelectric devices using nanoscale materials, in: 2007 IEEE Int. Electron Devices Meet, 2007. http://dx.doi10.1109/IEDM.2007.4418948.

[28] EH 4 GmbH. at http://www.micropelt.com/.

[29] B. Orr, A. Akbarzadeh, M. Mochizuki, R. Singh, A review of car waste heat recovery systems utilising thermoelectric generators and heat pipes, Appl. Therm. Eng. (2016), https://doi.org/10.1016/j.applthermaleng.2015.10.081.

[30] X. Chen, Y. Wang, L. Cai, Y. Zhou, Maximum power output and load matching of a phosphoric acid fuel cell-thermoelectric generator hybrid system, J. Power Sources (2015), https://doi.org/10.1016/j.jpowsour.2015.06.085.

[31] M. Zhao, H. Zhang, Z. Hu, Z. Zhang, J. Zhang, Performance characteristics of a direct carbon fuel cell/thermoelectric generator hybrid system, Energy Convers. Manage. 89 (2015) 683–689, https://doi.org/10.1016/j.enconman.2014.10.035.

[32] G.J. Snyder, Small thermoelectric generators, Electrochem. Soc. Interface (2008), https://doi.org/10.1109/ICT.2002.1190351.

[33] S. Priya, D.J. Inman, Energy harvesting technologies. Energy Harvesting Technologies, 2009. https://doi.org/10.1007/978-0-387-76464-1.

[34] A. Mehdizadeh Dehkordi, M. Zebarjadi, J. He, T.M. Tritt, Thermoelectric power factor: enhancement mechanisms and strategies for higher performance thermoelectric materials, Mater. Sci. Eng. R: Rep. (2015), https://doi.org/10.1016/j.mser.2015.08.001.

[35] R. Venkatasubramanian, E. Siivola, T. Colpitts, B. O'Quinn, Thin-film thermoelectric devices with high room-temperature figures of merit, Nature (2001), https://doi.org/10.1038/35098012.

[36] A.I. Hochbaum, R. Chen, R.D. Delgado, W. Liang, E.C. Garnett, M. Najarian, A. Majumdar, P. Yang, Enhanced thermoelectric performance of rough silicon nanowires, Nature (2008), https://doi.org/10.1038/nature06381.

[37] T.C. Harman, P.J. Taylor, M.P. Walsh, B.E. LaForge, Quantum dot superlattice thermoelectric materials and devices, Science (2002), https://doi.org/10.1126/science.1072886.

[38] B. Shen, R. Hendry, J. Cancheevaram, C. Watkins, M. Mantini, R. Venkatasubramanian. DC-DC converter suitable for thermoelectric generator, in: International Conference on Thermoelectrics, ICT, Proceedings, 2005. https://doi.org/10.1109/ICT.2005.1519999.

[39] S. Twaha, J. Zhu, Y. Yan, B. Li, K. Huang, Performance analysis of thermoelectric generator using dc-dc converter with incremental conductance based maximum power point tracking, Energy Sustain. Dev. (2017), https://doi.org/10.1016/j.esd.2017.01.003.

[40] M. He, F. Qiu, Z. Lin, Towards high-performance polymer-based thermoelectric materials, Energy Environ. Sci. (2013), https://doi.org/10.1039/c3ee24193a.

[41] J.P. Rojas, D. Singh, S.B. Inayat, G.T. Sevilla, H.M. Fahad, M.M. Hussain, Review—micro and nano-engineering enabled new generation of thermoelectric generator devices and applications, ECS J. Solid State Sci. Technol. (2017), https://doi.org/10.1149/2.0081703jss.

[42] J.H. Bahk, H. Fang, K. Yazawa, A. Shakouri, Flexible thermoelectric materials and device optimization for wearable energy harvesting, J. Mater. Chem. C (2015), https://doi.org/10.1039/c5tc01644d.

[43] K.A.A. Khalid, T.J. Leong, K. Mohamed, Review on thermionic energy converters, IEEE Trans. Electron Devices (2016), https://doi.org/10.1109/TED.2016.2556751.

[44] N.S. Rasor, Thermionic energy conversion plasmas, IEEE Trans. Plasma Sci. (1991), https://doi.org/10.1109/27.125041.

[45] V.S. Formenko, Handbook of Thermionic Properties, Springer, US, 1966, , https://doi.org/10.1007/978-1-4684-7293-6.

[46] S.M. Sze, K.L. Ng, Physics of Semiconductor Devices Physics of Semiconductor Devices. America, 1995. https://doi.org/10.1007/978-3-319-03002-9.

[47] V.S. Fomenko, Handbook of Thermionic Properties Electronic Work Functions and Richardson Constants of Elements and Compound, 1966.

[48] J.L. Lawless, S.H. Lam, An analytical model of thermionic discharges, J. Appl. Phys. (1986), https://doi.org/10.1063/1.336416.

[49] A.C. Marshall, An advanced thermionic theory: Recent developments, in: AIP Conference Proceedings, 2000. https://doi.org/10.1063/1.1290946.

[50] G.D. Mahan, L.M. Woods, Multilayer thermionic refrigeration, Phys. Rev. Lett. (1998), https://doi.org/10.1103/PhysRevLett. 80.4016.

[51] F. Morini, E. Dubois, J.F. Robillard, S. Monfray, T. Skotnicki, Low work function thin film growth for high efficiency thermionic energy converter: coupled Kelvin probe and photoemission study of potassium oxide, Phys. Status Solidi (A) Appl. Mater. Sci. (2014), https://doi.org/10.1002/pssa.201300136.

[51a] V. Giorgis, F. Morini, T. Zhu, J.F. Robillard, X. Wallart, J.L. Codron, E. Dubois, Synthesis and characterization of low work function alkali oxide thin films for unconventional thermionic energy converters, J. Appl. Phys. 120 (20) (2016), https://doi.org/10.1063/1.4968532.

[52] G.N. Hatsopoulos, E.P. Gyftopoulos, Thermionic energy conversion, in: Vol. 1: Processes and Devices: Solar Energy Materials and Solar Cells, 2014. https://doi.org/10.1016/j.solmat.2013.11.008.

[53] G. Hatsopoulos, Transport effects in cesium thermionic converters, Proc IEEE (1963), https://doi.org/10.1109/PROC.1963.2265.

[54] G.N. Hatsopoulos, J. Kaye, Measured thermal efficiencies of a diode configuration of a thermo electron engine, J. Appl. Phys. (1958), https://doi.org/10.1063/1.1723373.

[55] S. Meir, C. Stephanos, T.H. Geballe, J. Mannhart, Highly-efficient thermoelectronic conversion of solar energy and heat into electric power, J. Renew. Sustain. Energy (2013), https://doi.org/10.1063/1.4817730.

[56] J.H. Lee, I. Bargatin, K. Iwami, K.A. Littau, M. Vincent, R. Maboudian, Z.X. Shen, N.A. Melosh, R.T. Howe, Encapsulated thermionic energy converter with stiffened suspension, Solid-State Sensors, Actuators, and Microsystems Workshop, 2012.

[57] P.A. Anderson, The work function of lithium, Phys. Rev. (1949), https://doi.org/10.1103/PhysRev. 75.1205.

[58] H.B. Michaelson, The work function of the elements and its periodicity, J. Appl. Phys. (1977), https://doi.org/10.1063/1.323539.

[59] J.J. Uebbing, L.W. James, Behavior of cesium oxide as a low work-function coating, J. Appl. Phys. (1970), https://doi.org/10.1063/1.1658489.

[60] J.X. Wu, M.S. Ma, J.S. Zhu, M.R. Ji, The interaction of cesium-oxide overlayers with Ge(1 1 1) as a function of annealing temperature, Appl. Surf. Sci. 173 (2001) 8–14, https://doi.org/10.1016/S0169-4332(00)00854-0.

[61] S. Kim, M.Y. Lee, S. Lee, S.H. Jhi, Super low work function of alkali-metal-adsorbed transition metal dichalcogenides, J. Phys.: Condens. Matter (2017), https://doi.org/10.1088/1361-648X/aa79bd.

[62] J.I. Lee, Y.H. Jeong, H.C. No, R. Hannebauer, S.K. Yoo, Size effect of nanometer vacuum gap thermionic power conversion device with CsI coated graphite electrodes, Appl. Phys. Lett. (2009), https://doi.org/10.1063/1.3266921.

[63] S. Basu, Z.M. Zhang, C.J. Fu, Review of near-field thermal radiation and its application to energy conversion, Int. J. Energy Res. (2009), https://doi.org/10.1002/er.1607.

[64] R.Y. Belbachir, Z. An, T. Ono, Thermal investigation of a micro-gap thermionic power generator, J. Micromech. Microeng. (2014), https://doi.org/10.1088/0960-1317/24/8/085009.

[65] H. Yuan, D.C. Riley, Z.X. Shen, P.A. Pianetta, N.A. Melosh, R.T. Howe, Back-gated graphene anode for more efficient thermionic energy converters, Nano Energy (2017), https://doi.org/10.1016/j.nanoen.2016.12.027.

[66] G. Xiao, G. Zheng, M. Qiu, Q. Li, D. Li, M. Ni, Thermionic energy conversion for concentrating solar power, Appl. Energy (2017), https://doi.org/10.1016/j.apenergy.2017.09.021.

[67] Y. Hishinuma, T.H. Geballe, B.Y. Moyzhes, T.W. Kenny, Measurements of cooling by room-temperature thermionic emission across a nanometer gap, J. Appl. Phys. (2003), https://doi.org/10.1063/1.1606852.

[68] M. Zebarjadi, Solid-state thermionic power generators: an analytical analysis in the nonlinear regime, Phys. Rev. Appl. (2017), https://doi.org/10.1103/PhysRevApplied. 8.014008.

[69] L. Ju, J. Velasco Jr, E. Huang, S. Kahn, C. Nosiglia, H.Z. Tsai, W. Yang, T. Taniguchi, K. Watanabe, Y. Zhang, G. Zhang, Photoinduced doping in heterostructures of graphene and boron nitride, Nat. Nanotechnol. (2014), https://doi.org/10.1038/nnano.2014.60.

[70] H.J. Goldsmid, Review of thermoelectric materials, Introduction to Thermoelectricity, Springer, Berlin, Heidelberg, 2016, pp. 153–195, , https://doi.org/10.1007/978-3-662-49256-7.

[71] J.W. Schwede, I. Bargatin, D.C. Riley, B.E. Hardin, S.J. Rosenthal, Y. Sun, F. Schmitt, P. Pianetta, R.T. Howe, Z.X. Shen, N.A. Melosh, Photon-enhanced thermionic emission for solar concentrator systems, Nat. Mater. (2010), https://doi.org/10.1038/nmat2814.

[72] P. Shefsiek, Describing and correlating the performance of the thermionic converter: a historical perspective, IEEE Trans. Plasma Sci. (2010), https://doi.org/10.1109/TPS.2010.2050910.

[73] S.B. Lang, Pyroelectricity: from ancient curiosity to modern imaging tool, Phys. Today (2005), https://doi.org/10.1063/1.2062916.

[74] S.B. Lang, Sourcebook of Pyroelectricity, CRC Press, 1974.

[75] C.R. Bowen, J. Taylor, E. LeBoulbar, D. Zabek, A. Chauhan, R. Vaish, Pyroelectric materials and devices for energy harvesting applications, Energy Environ. Sci. (2014), https://doi.org/10.1039/C4EE01759E.

[76] G. Sebald, D. Guyomar, A. Agbossou, On thermoelectric and pyroelectric energy harvesting, Smart Mater. Struct. (2009), https://doi.org/10.1088/0964-1726/18/12/125006.

[77] C.R. Bowen, H.A. Kim, P.M. Weaver, S. Dunn, Piezoelectric and ferroelectric materials and structures for energy harvesting applications, Energy Environ. Sci. (2014), https://doi.org/10.1039/c3ee42454e.

[78] C.R. Bowen, J. Taylor, E. Le Boulbar, D. Zabek, V.Y. Topolov, A modified figure of merit for pyroelectric energy harvesting, Mater. Lett. (2015), https://doi.org/10.1016/j.matlet.2014.10.004.

[79] X. Li, S.G. Lu, X.Z. Chen, H. Gu, X.S. Qian, Q.M. Zhang, Pyroelectric and electrocaloric materials, J. Mater. Chem. C (2013), https://doi.org/10.1039/c2tc00283c.

[80] S.B. Lang, S. Muensit, Review of some lesser-known applications of piezoelectric and pyroelectric polymers, Appl. Phys. A Mater. Sci. Process. (2006), https://doi.org/10.1007/s00339-006-3688-8.

[81] M. Vaish, M. Sharma, R. Vaish, V.S. Chauhan, experimental study on waste heat energy harvesting using lead zirconate titanate (PZT-5H) pyroelectric ceramics, Energy Technol. (2015), https://doi.org/10.1002/ente.201500050.

[82] M.D. Aggarwal, A.K. Batra, P. Guggilla, M.E. Edwards, D. Garcia, Pyroelectric Materials for Uncooled Infrared Detectors: Processing, Properties, and Applications, Technical report 2010, Natl. Aeronaut. Sp. Adm. 2010.

[83] D.U.P. Spinola, E.N. Moreira, L.A. Bassora, J.A. Eiras, D. Garcia, Pyroelectric and piezoelectric properties of SBN ceramics, 1996 IEEE Ultrason. Symp. Proc. 1996, pp. 523–526, , https://doi.org/10.1109/ULTSYM.1996.584029.

[84] A. Cuadras, M. Gasulla, V. Ferrari, Thermal energy harvesting through pyroelectricity, Sensors Actuators, A Phys. (2010), https://doi.org/10.1016/j.sna.2009.12.018.

[85] Y. Yang, W. Guo, K.C. Pradel, G. Zhu, Y. Zhou, Y. Zhang, Y. Hu, L. Lin, Z.L. Wang, Pyroelectric nanogenerators for harvesting thermoelectric energy, Nano Lett. (2012), https://doi.org/10.1021/nl3003039.

[86] D. Zabek, J. Taylor, C.R. Bowen, Characterization and modeling of meshed electrodes on free standing polyvilylidene difluoride (PVDF) films for enhanced pyroelectric energy harvesting, IEEE Trans. Ultrason. Ferroelectr. Freq. Control (2016), https://doi.org/10.1109/TUFFC.2016.2606127.

[87] Y. Yang, S. Wang, Y. Zhang, Z.L. Wang, Pyroelectric nanogenerators for driving wireless sensors, Nano Lett. (2012), https://doi.org/10.1021/nl303755m.

[88] L. Kouchachvili, M. Ikura, Improving the efficiency of pyroelectric conversion, Int. J. Energy Res. (2008), https://doi.org/10.1002/er.1361.

[89] S. Bhattacharjee, A.K. BatrA, J. Cain, Carbon nano fiber reinforced cement composite for energy harvesting road, Green Streets Highw. ASCE 2011 (2011), https://doi.org/10.1061/41148(389)22.

[90] A.K. Batra, Simulation of energy harvesting from roads via pyroelectricity, J. Photonics Energy (2011), https://doi.org/10.1117/1.3656395.

[91] S. Mohammadi, A. Khodayari, Free energy harvesting from ambient temperature variations, Int. J. Mech. Mater Eng. (2011).

[92] M. Sharma, A. Chauhan, R. Vaish, V.S. Chauhan, Pyroelectric materials for solar energy harvesting: a comparative study, Smart Mater. Struct. (2015), https://doi.org/10.1088/0964-1726/24/10/105013.

[93] A.E. Beasley, C.R. Bowen, D.A. Zabek, C.T. Clarke, Use it or lose it: the influence of second order effects of practical components on storing energy harvested by pyroelectric effects, tm-Tech. Mess. 85 (9) (2018) 533, https://doi.org/10.1515/teme-2017-0075.

[94] S.K.T. Ravindran, T. Huesgen, M. Kroener, P. Woias, A self-sustaining micro thermomechanic-pyroelectric generator, Appl. Phys. Lett. (2011), https://doi.org/10.1063/1.3633350.

[95] R.B. Olsen, J.M. Briscoe, D.A. Bruno, W.F. Butler, A pyroelectric energy converter which employs regeneration, Ferroelectrics (1981), https://doi.org/10.1080/00150198108209595.

[96] J. Fang, H. Frederich, L. Pilon, Harvesting nanoscale thermal radiation using pyroelectric materials, J. Heat Transfer (2010), https://doi.org/10.1115/1.4001634.

[97] Zeyu Zhang, Brendan Hanrahan, Chuan Shi, A. Khaligh, Management and storage of energy converted via a pyroelectric heat engine, Appl. Energy 230 (2018) 1326–1331, https://doi.org/10.1016/j.apenergy.2018.09.101.

[98] G. Cha, Y.S. Ju, Pyroelectric energy harvesting using liquid-based switchable thermal interfaces, Sensors Actuators, A Phys. (2013), https://doi.org/10.1016/j.sna.2012.09.019.

[99] S.R. Hunter, N.V. Lavrik, S. Mostafa, S. Rajic, P.G. Datskos, Review of pyroelectric thermal energy harvesting and new MEMs based resonant energy conversion techniques, in: Proceedings of SPIE – The International Society for Optical Engineering, 2012. https://doi.org/10.1117/12.920978.

[100] Y. Bai, T. Siponkoski, J. Peräntie, H. Jantunen, J. Juuti, Ferroelectric, pyroelectric, and piezoelectric properties of a photovoltaic perovskite oxide, Appl. Phys. Lett.

(2017), https://doi.org/10.1063/1.4974735.

[101] J.H. Lee, et al., Highly stretchable piezoelectric-pyroelectric hybrid nanogenerator, Adv. Mater. (2014), https://doi.org/10.1002/adma.201303570.

[102] B. Bhatia, H. Cho, J. Karthik, J. Choi, D.G. Cahill, L.W. Martin, W.P. King, High Power Density Pyroelectric Energy Conversion in Nanometer-Thick BaTiO$_3$ Films, Nanoscale Microscale Thermophys. Eng. (2016), https://doi.org/10.1080/15567265.2016.1252820.

[103] M. Xie, D. Zabek, C. Bowen, M. Abdelmageed, M. Arafa, Wind-driven pyroelectric energy harvesting device, Smart Mater. Struct. (2016), https://doi.org/10.1088/0964-1726/25/12/125023.

[104] R.A. Kishore, S. Priya, A review on design and performance of thermomagnetic devices, Renew. Sustain. Energy Rev. (2018), https://doi.org/10.1016/j.rser.2017.07.035.

[105] M. Ujihara, G.P. Carman, D.G. Lee, Thermal energy harvesting device using ferromagnetic materials, Appl. Phys. Lett. (2007), https://doi.org/10.1063/1.2775096.

[106] L.D. Kirol, J.I. Mills, Numerical analysis of thermomagnetic generators, J. Appl. Phys. (1984), https://doi.org/10.1063/1.334015.

[107] D. Solomon, Design of a thermomagnetic generator, Energy Convers. Manage. (1991), https://doi.org/10.1016/0196-8904(91)90068-T.

[108] J.F. Elliott, Thermomagnetic generator, J. Appl. Phys. (1959), https://doi.org/10.1063/1.1735054.

[109] C.J. Hsu, S.M. Sandoval, K.P. Wetzlar, G.P. Carman, Thermomagnetic conversion efficiencies for ferromagnetic materials, J. Appl. Phys. (2011), https://doi.org/10.1063/1.3672844.

[110] H.E. Nigh, S. Legvold, F.H. Spedding, Magnetization and electrical resistivity of gadolinium single crystals, Phys. Rev. (1963), https://doi.org/10.1103/PhysRev.132.1092.

[111] K.B. Joshi, S. Priya, Multi-physics model of a thermo-magnetic energy harvester, Smart Mater. Struct. (2013), https://doi.org/10.1088/0964-1726/22/5/055005.

[112] S.M. Sandoval, A.E. Sepulveda, S.M. Keller, On the thermodynamic efficiency of a nickel-based multiferroic thermomagnetic generator: from bulk to atomic scale, J. Appl. Phys. (2015), https://doi.org/10.1063/1.4919354.

[113] A. Post, C. Knight, E. Kisi, Thermomagnetic energy harvesting with first order phase change materials, J. Appl. Phys. (2013), https://doi.org/10.1063/1.4815933.

[114] V. Srivastava, Y. Song, K. Bhatti, R.D. James, The direct conversion of heat to electricity using multiferroic alloys, Adv. Energy Mater. (2011), https://doi.org/10.1002/aenm.201000048.

[115] Y. Song, Performance analysis of energy conversion via caloric effects in first-order ferroic phase transformations, PCCP (2014), https://doi.org/10.1039/c4cp00938j.

[116] Greg P. Carman, Kyle Wetzlar, Ray Hsu, S. Sandoval, Energy Harvesting A Nano-Scale Based Magneto-Thermal-Electric Element, 2015.

[117] T. Christiaanse, E. Brück, Proof-of-concept static thermomagnetic generator experimental device, Metall. Mater. Trans. E (2014), https://doi.org/10.1007/s40553-014-0006-9.

[118] J. Chun, H.C. Song, M.G. Kang, H.B. Kang, R.A. Kishore, S. Priya, Thermo-magneto-electric generator arrays for active heat recovery system, Sci. Rep. (2017), https://doi.org/10.1038/srep41383.

[119] C.C. Chen, T.K. Chung, C.Y. Lin, A novel thermomagnetic-Actuated gripper with a piezoelectric-pyroelectric sensing readout of gripping states and forces, IEEE Trans. Magn. (2017), https://doi.org/10.1109/TMAG.2017.2731320.

[120] M. Gueltig, F. Wendler, H. Ossmer, M. Ohtsuka, H. Miki, T. Takagi, M. Kohl, High-performance thermomagnetic generators based on heusler alloy films, Adv. Energy Mater. (2017), https://doi.org/10.1002/aenm.201601879.